Time-resolved x-ray fluorescence of He-like ions in an aluminum-laser-produced plasma

P. Renaudin, C. Chenais-Popovics, and J. C. Gauthier
Laboratoire pour l'Utilisation des Lasers Intenses, Ecole Polytechnique, 91128 Palaiseau, France

O. Peyrusse
Centre d'Etudes de Limeil-Valenton, 94195 Villeuneuve St. Georges Cedex, France

C. A. Back
Lawrence Livermore National Laboratory, Livermore, California 94550
(Received 14 February 1994)

Quasiresonant photoexcitation and nonresonant photoionization of He-like ions in a two-component laser-produced plasma are demonstrated in the x-ray range. The pumping source is the x-ray emission of a high-Z plasma which modifies the populations of the excited states of an aluminum He-like plasma. Fluorescence of the $1s2p$-$1s^2$ line at 7.757 Å has been measured by time-resolved and time-integrated spectral measurements of the two plasma emissions. Photoionization results compare favorably with radiative transfer simulations which calculate the He-like $1s2p$-$1s^2$ line transfer in the photopumped aluminum plasma.

PACS number(s): 52.20.−j, 52.25.Jm, 52.50.−b, 52.25.Nr

I. INTRODUCTION

Radiative transfer in a laser-produced plasma has been studied as part of the inertial confinement function and x-ray laser research. X-ray emission induced by excitation of given transitions in a laser-produced plasma can be used to study ionization or excitation dynamics of one or several radiative transitions in the plasma. Such investigation has been proposed and demonstrated [1–3] in the past few years, in particular on a resonant He-like aluminum scheme [4,5].

The study of fluorescence resulting from a radiative pump opens a new area for plasma spectroscopy. Such active spectroscopy can be used as a probe for radiative transfer studies. The induced fluorescence gives information about radiative processes, nonlocal-thermodynamic-equilibrium (NLTE) population kinetics, and ionization balance in the pumped plasma. Fundamental studies of the ionization and excitation dynamics of one or several radiative transitions of the plasma can be performed with this technique [6]. Photopumping has also been proposed to produce [7–13] or enhance population inversion in x-ray laser schemes [2,14–15] and has been put forward as a possible diagnostic of core-shell mixing in a spherical plasma implosion [16].

The organization of the paper is as follows. The description and the optimization of all the important parameters of the photopumping experiment are presented in Sec. II. The schemes chosen for the present study are also described in this section. In Sec. III are presented the experimental system and the target design. A more detailed description of the experimental alignment precision required in this type of experiment will be given here. Section IV presents the full three-beam photopumping experiment and the principal results. A detailed simulation of the experiment is undertaken in Sec. V. The approach used here is to perform a detailed radiation-transfer calculation that can predict the fluorescence levels of the transitions of interest. Section VI presents the conclusions.

II. DESCRIPTION AND OPTIMIZATION OF PHOTOPUMPING EXPERIMENTS

In the present work, we have driven two different experiments using a nonresonant and a quasiresonant photopumping scheme. In the two cases, the pumping source is the broadband emission of a high-Z plasma and the photopumped medium is an aluminum He-like dominant plasma. For the nonresonant and quasiresonant pumping, the x-ray source respectively photoionizes and photoexcites the aluminum plasma. The advantages of using a broadband pumping spectrum in comparison to a line coincidence scheme [5] are twofold. First, the difficulty of finding a good coincidence taking account of line shifts is avoided. Second, the emission of the pump can be spectrally decoupled from the fluorescence and the signal obtained is more easily distinguished from the pump in the observed spectrum.

In our experiment, we have chosen He-like ions which can be produced at relatively low temperatures (150–200 eV). Because the He-like ions have a closed shell, it is possible to create a He-like plasma during a long time after the maximum of the laser pulse. To have efficient photopumping, the majority of the ions present in the plasma must be in the ground state. This is verified in the case of He-like ions because the excitation energy of the $1s2p$ level is very much higher than the ground state energy.

The experimental geometry chosen for these photopumping experiments is based on two plasmas produced by laser beams focused on each side of a multilayered tar-

get. Figure 1 shows the setup of the diagnostics and the target configuration. For the photoexcitation scheme, the intense emission of a Ba plasma is used to pump the $1s2p$-$1s^2$ resonance line of Al XII at 7.757 Å. In the photoionization scheme, the M-band emission of tungsten is used to photoionize the $1s^2$ level of Al XII. In the two cases, the fluorescence of Al He-like lines is expected. Collisional-radiative calculations show that the strongest fluorescence of the K-shell emission lines is obtained with the $1s2p$-$1s^2$ He_α resonance line because of its strong oscillator strength [17].

Figure 2(a) shows the level diagram of the Al He-like ion together with the two x-ray pumping mechanisms. Only the levels relevant to the present experimental situation are represented. Three-body recombination is the dominant decay mechanism which populates the upper excited states of the photoionized ion. Radiative cascades follow and drive the fluorescence of the He-like resonance lines. In the photoexcitation scheme, a direct population transfer to the $1s2p$ level is followed by the spontaneous emission of the He_α resonance line. If the photoexciting x-ray source spectrum is broad enough, it is possible to photoexcite all the excited levels of the He-like ion. Population inversions are obtained due to recombination cascades in the photoionization case or due to direct population transfer in the photoexcitation case. This fact probably induced a strong emission of the Balmer series lines. However, they appear in a spectral range which cannot be measured with the present instrumentation.

Figure 2(b) shows different experimental spectra of barium and tungsten obtained with a laser intensity of 5×10^{14} W/cm^2. An Al He-like and H-like spectrum is superimposed to provide a spectral reference. As can be seen from Fig. 2(b), the $3d$-$4f$ unresolved transition array (UTA) emission of tungsten is a 200 eV width broadband emission. A good overlap of this emission with the Al He-like ionization limit at 2086 eV is observed. The W emission is two times greater than the Ba emission in the same energy range (2000–2200 eV). On the other hand, the Ba emission around 1600 eV is more efficient to photoexcite the ground state and to populate the $1s2p$ level: it is three times greater than the W emission. The observed Ba emission at the Al H-like ionization limit (2300 eV) is weak.

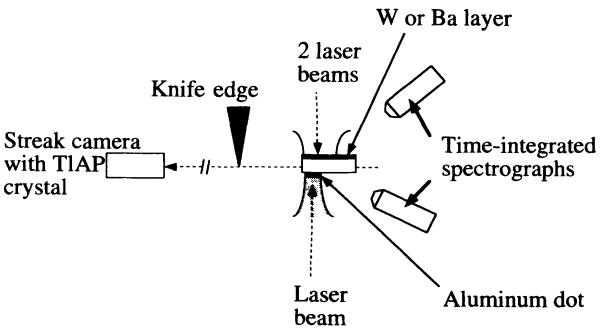

FIG 1. Photopumping experimental geometry. Time-resolved spectrum of the two plasmas are recorded by a streak camera fitted with a thallium hydrogen phthalate (TIAP) flat crystal.

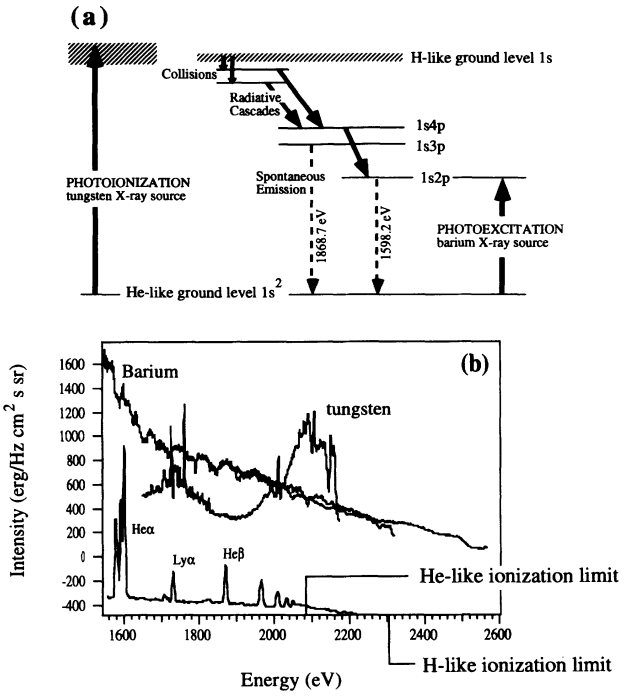

FIG. 2. (a) Level scheme of the He-like aluminum ions with the ionization pumping and the excitation pumping. (b) Time-integrated spectra of tungsten and barium plasmas [intensity 5×10^{14} W/cm^2, full width at half maximum (FWHM) 600 ps, wavelength 0.53 μm] shown with the K-shell emission of an aluminum plasma.

Previous numerical simulations and experiments have been performed to optimize the creation of the two plasmas [18]. Collisional-radiative simulations have been used to determine the optimal conditions which maximize the fluorescence of the Al He_α line in the photoionization case. The principal results of the simulations were the following.

(a) The optimal plasma conditions are a temperature of 100–200 eV and an electron density of 5×10^{21} cm^{-3}.

(b) The best x-ray source to photoionize the aluminum plasma is the $3d$-$4f$ lines of tungsten compared to other materials with neighboring atomic numbers such as tantalum ($Z=73$) and rhenium ($Z=75$). This is due to the better overlap of the $3d$-$4f$ UTA emission of tungsten with the Al He-like recombination continuum as noted earlier.

(c) The highest fluorescence signal of the K-shell emission lines is obtained with the He_α line because of its greater oscillator strength.

(d) Fluorescence appears closer to the target than self-emission because the absorption of the photopumping radiation of tungsten is very high in the densest part of the aluminum plasma in our target design (0.1 μm absorption length for 5×10^{21} cm^{-3} electronic density).

(e) The reabsorption of the He_α resonance line being important, microdot targets have to be used to reduce the lateral density and temperature gradients.

The two plasmas were created with laser parameters that were determined from preliminary experiments. First, the laser intensity which creates the Al plasma with a minimum emission of the $1s2p$-$1s^2\ ^1S_0$ line in the time-resolved spectrograph has been determined to be 5×10^{12} W/cm^2. To obtain a maximum photopumping x-ray intensity, the thickness of the aluminum dot and the high-Z element layer were chosen to be completely ablated during the laser pulses. With a laser intensity of 5×10^{12} W/cm^2, this aluminum dot thickness has been measured to be 3000 Å. For these conditions, the peak of the laser beam that created the x-ray source must be delayed by 600 ps relative to the peak of the first laser pulse. This delay is necessary to obtain a He-like aluminum plasma fitting the optimum electronic temperature and density gradients deduced from calculations. Concerning the pump plasma, 700 Å of tungsten or 4000 Å of BaF_2 were ablated for a laser intensity of 5×10^{14} W/cm^2.

Other experiments have been performed to measure the x-ray flux transmitted through different substrates. The best compromise between high transmission and target fabrication has been found to be a 10 μm polypropylene (CH) foil.

III. EXPERIMENTAL SYSTEM AND TARGET DESIGN

All these results determine the optimal conditions for the laser parameters and the target geometry. The experiments were performed at the LULI facility at Palaiseau (France) using three laser beams. The laser pulse durations were equal to 600 ps for the three beams. The targets consisted of a 10 μm thick polypropylene substrate with a microdot of 100 or 200 μm diameter of aluminum and a layer of tungsten or barium (see Fig. 1). The dot, a 3000 or 4000 Å thick spot of aluminum, was irradiated by a 600 ps beam of 0.53 μm wavelength to create the plasma. A homogeneous 300 μm diameter focal spot, greater than the aluminum dot, was obtained by focusing the laser beam passing through a random phase plate. A relatively low irradiance of 5×10^{12} W/cm^2 was used to prepare it in the He-like ion ground state. This was obtained with a laser energy of about 2 J.

The high-Z layer (700 Å of tungsten or 4000 Å of BaF_2) was irradiated by the two other beams to create the x-ray source. A 0.53 μm wavelength laser beam at an irradiance of 5×10^{14} W/cm^2 was used to enhance the x-ray conversion efficiency of the pumping source. A diameter of 200 μm for the x-ray source was obtained by the use of two superimposed laser beams. The x-ray flux in the $3d$-$4f$ lines was equal to 4×10^{12} W/cm^2.

The fabrication and alignment of the targets were a key point for these experiments. To reduce the reabsorption along the line of view, the two plasmas were not aligned exactly center to center. The irradiation on the high-Z layer was adjusted on the foil edge as shown in Fig. 1.

Temporal resolution of the Al He_α emission signal is another key point to distinguish fluorescence from other emission mechanisms. So, the fluorescence was recorded by a time-resolved spectrograph, consisting of a streak camera coupled with a TIAP (thallium hydrogen phthalate) flat crystal. The streak camera viewed the target at 90° from the target normal. A CsI cathode was used on the streak camera. Its high sensitivity was important here as the fluorescence signal is weak. A disadvantage of the CsI cathode is that its sensitivity is not well known because it suffers from aging problems. That means first that the cathode efficiency varies significantly from shot to shot and second that this efficiency is not uniform on the whole photocathode.

The emission from the x-ray source was blocked by a knife edge carefully aligned with the target by a microscope. This alignment ensured that the streak camera was blocked from the pump plasma but could still record the aluminum emission. Because the fluorescence was expected in the densest part of the plasma close to the target surface, the position of the knife edge was set at the limit where the x-ray source was directly seen by the streak camera. Two time-integrated spectrometers used flat PET (pentaerythritol) crystals to monitor the spectral emission of the two plasmas on either side of the target. They covered a wavelength range of 5.5–8 Å and measured the x-ray source emission and substrate absorption. A pinhole camera monitored the focal spot and the dot position.

IV. FLUORESCENCE EXPERIMENTS

Fluorescence of the Al He_α line has been evidenced by measuring the temporal evolution of the aluminum emission during the photopumping process with the time-resolved spectrograph. First, we checked that, when only the pumped plasma was created with the optimal laser intensity of 5×10^{12} W/cm^2, no Al XII resonance lines were visible because the He-like ions were created in the ground state and the He_α line self-emission was lower than the camera threshold for this laser intensity. The time delay between the laser beams has been adjusted to 600 ps by measuring the emission of the Al XII resonance lines and the high-Z plasma on the streak camera. This was done with shots on the multilayered targets with higher laser flux on the aluminum side and without the knife edge.

Figure 3(a) shows the time-resolved emission of the aluminum plasma and the M-band tungsten plasma emission recorded in optimal photoionization conditions. This was obtained with the target scheme shown in Fig. 1, the pump W plasma being produced by two laser beams focused into a 150 μm diameter focal spot.

Early in time, no self-emission of aluminum can be seen during the pump laser pulse, as in the shots without photopumping first mentioned in this section. For this shot, the knife edge did not hide completely the tungsten plasma emission to be sure that the aluminum fluorescence zone was viewed by the streak camera, so a W spectrum appears in Fig. 3(a). At 7.757 Å, an enhancement of the Al XII He_α line emission can be seen on top of the weak W emission. One can note that this signal appears exactly during the tungsten emission.

Some shots were performed on the tungsten layer only, in the same conditions as in the shot shown in Fig. 3(a), but without shooting the laser beam on the Al side. Figure 3(b) shows the time-resolved spectrum of the tungsten

plasma obtained. One can see that tungsten emits no line at 7.757 Å, the wavelength of the He_α line. The comparison of Figs. 3(a) and 3(b) clearly shows that the Al He_α line is emitting only during the pumping process.

To correct the fluorescence data, the region at 7.757 Å in the spectrum of Fig. 3(b) was normalized to the spectrum of Fig. 3(a) and subtracted from the fluorescence signal. Figure 4 shows a densitometer trace of the Al He_α line emission as a function of time. It shows a quite visible fluorescence signal whose intensity can be evaluated (even if not absolutely measured) due to the uncertainty of the streak camera sensitivity. It is on the order of a few times the streak camera threshold, which is estimated to be a few 10^9 W/cm^2 by comparison with time-integrated spectrograph data. On each shot, the pump spectrum was recorded with the time-integrated spectrographs to have a measurement of x-ray flux of the pump plasma. The fluorescence signal is then evaluated to a few 10^{-4} of the x-ray pump intensity.

The fluorescence has been recorded only when the aluminum dot was well aligned on the edge of the foil target, due to the critical importance of the reabsorption of the line along the line of sight of the spectrograph. The fluorescence of the He_α line was seen on several shots, for 300 and 400 nm thick dots, but not for 200 nm thick ones. This minimum thickness and the fact that the fluorescence signal has not been observed when the knife edge was so close to the target as to hide completely the W spectrum show that the fluorescence region is close to the target.

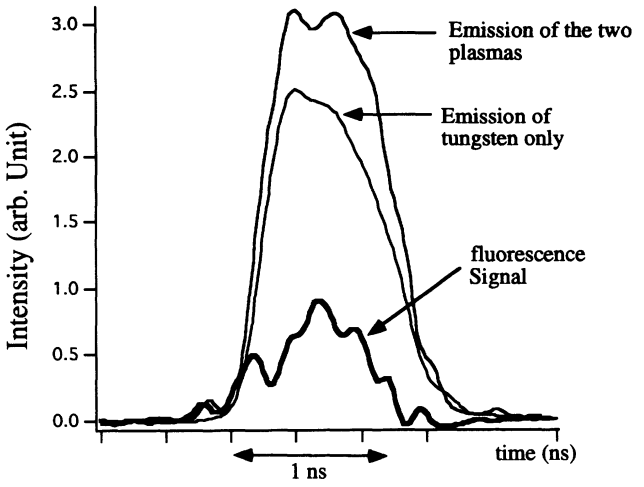

FIG. 4. Densitometer trace of 100 mÅ wide around the He_α fluorescence signal as a function of time from Figs. 3(a) and 3(b). Tungsten emission of Fig. 3(b) is renormalized and subtracted from the emission of Fig. 3(a). The fluorescence signal is seen only during the x-ray pump duration. The multilayer target is 10 μm thick CH with a 3000 Å thick Al microdot of 100 μm and 700 Å thick W.

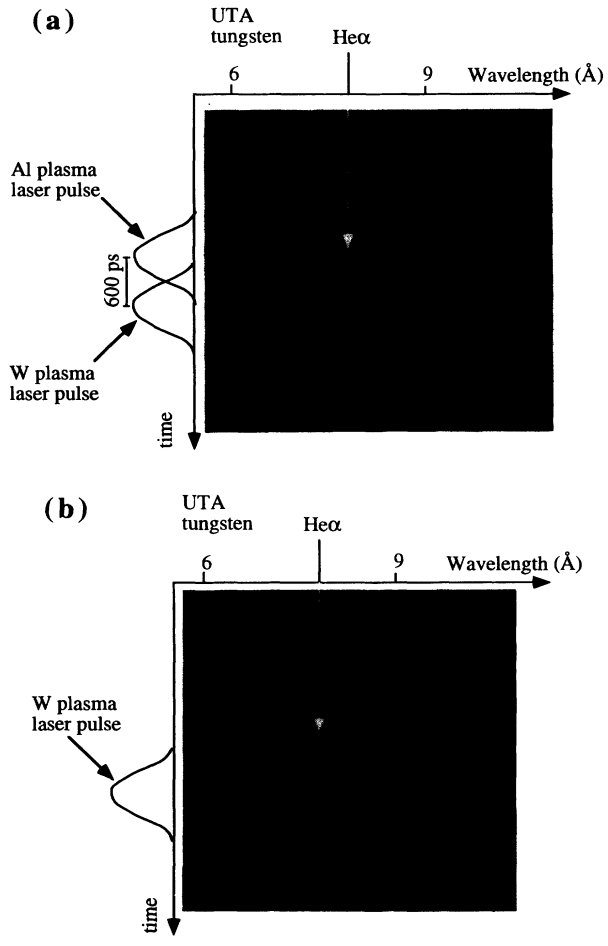

FIG. 3. (a) Time-resolved spectrum of the two plasmas showing the fluorescence of the He_α line; (b) time-resolved spectrum of the tungsten plasma only (laser intensity 10^{14} W/cm^2, FWHM 600 ps, wavelength 0.53 μm).

Similar results were obtained in the photoexcitation experiments with a Ba pump by irradiating in the same laser conditions a 400 nm Ba layer. As in the photoionization case, the Al He_α emission line was recorded only during the pump laser duration by the streak camera. The Ly_α line was also exhibiting a weak fluorescence signal at the same time with the same duration. The fact that the Ly_α line also appears is probably due to the wide spectrum of barium, which can photoexcite the whole He-like Rydberg series, and also the Ly_α line. In the photoionization case, even if the Ly_α fluorescence occurred, it would not be observed because the $3d$-$4p$ lines of tungsten overlap the wavelength of the aluminum Ly_α line.

Finally, a few shots have been done with a samarium pump. This was done in order to check that the Al He_α line emission could not be due to a shock or radiative heating of the Al layer, the samarium spectrum being weak in the photoionizing and photoexciting spectral range (less than 300 erg/Hz cm^2 s sr). No Al emission lines have been observed in this case.

V. NUMERICAL SIMULATIONS AND ANALYSIS OF THE EXPERIMENTS

To compare the results obtained in these two experimental series and to better understand the reabsorption mechanisms, we did some simulations of these experi-

ments. The non-LTE atomic level population distribution in the photoionized or photoexcited aluminum plasma has been simulated with the TRANSPEC code, a one-dimensional plasma radiation-dependent collisional-radiative model for *K*-shell spectroscopy [19]. This model is time dependent and is used here as a postprocessor of the one-dimensional Lagrangian hydrocode FILM [20]. The coupling of radiation with the populations is self-consistently obtained in an iterative way in which populations are obtained by linerization while the line transfer can be computed within the core saturation approximation.

The input hydrodynamic file was calculated with FILM. The pulse duration was 600 ps at 0.53 μm wavelength with a laser intensity of 5×10^{12} W/cm^2. The electron conduction is modeled by a delocalized flux model [21].

The x-ray pump was a digitized experiment spectrum between 2000 and 2200 eV for tungsten and between 1600 and 2300 eV for barium as shown in Fig. 2(b). Its temporal behavior was modeled as a 600 ps Gaussian pulse delayed by 600 ps after the maximum of the laser pulse creating the Al plasma.

Absorption of the x rays from the source in the target and reabsorption of the Al XII resonance lines along the observation axis were taken into account. The radiative-transfer equation was solved in each cell for each transition, taking into account its line profile. The temporal evolution of the line emission was obtained with a given finite transversal dimension of the plasma, 100 μm in our case, i.e., the dot dimension.

Figure 5 shows the time evolution of the aluminum and the photoionization tungsten source emissions as seen from the aluminum side. Aluminum resonance lines appear as emission or absorption structures in the tungsten spectrum. One can note that the He$_\alpha$ line is very emissive. The fact that the H-like emission remains weak indicates that the pumped plasma is in an optimal state that maximizes the photopumping mechanism. The high ratio between the He$_\alpha$ line and the other resonance lines is in accordance with the fact that in the photoionization experiment we see only the fluorescence of the He$_\alpha$ line, whose intensity is close to the streak camera threshold.

With the TRANSPEC code, we can also compare the time evolution of the aluminum plasma emissivity obtained with two different x-ray sources. Figure 6 shows the time evolution of the He$_\alpha$ line obtained without photopumping and with the tungsten photoionizing and the barium photoexciting x-ray source. As a consequence of the photopumping, an enhancement of the line emission is evident. The delay between the fluorescence signal and the self-emission is equal to the delay between the peaks of the two laser pulses. The fluorescence signal shown in Fig. 6 compares well on the whole to the experimental data shown in Figs. 3 and 4.

We can analyze in more detail the intensities and delays in Fig. 6. The emissivity of the fluorescence is roughly the same with the two different x-ray sources. We can see that the peak of self-emission (without photopumping) is about a factor of 7 lower than the peak of the fluorescence (with photopumping). The fluorescence due to Ba occurs at the same time as the fluorescence due to W. This is due to the fact that, in the photoionization scheme, the collisional recombination is so fast that it induces no detectable additional delay.

A small discrepancy appears in the comparison of the experimental data and the simulations: the He$_\alpha$ line emission is observed exactly during the laser irradiation of the W layer in the experiment, and it appears 300 ps later in the simulation. This time delay between fluorescence and the x-ray pump can be explained by a small discrepancy in the calculated and experimental Al ablation depth which modifies the x-ray pump absorption

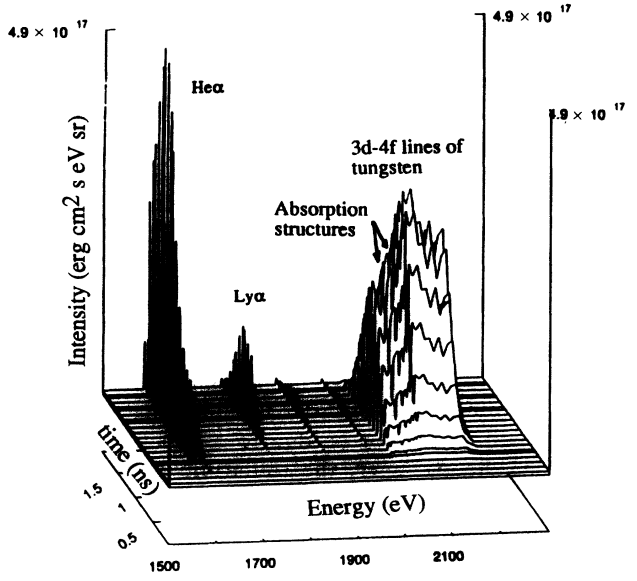

FIG. 5. Time-dependent evolution of the 3*d*-4*f* band emission of tungsten plasma (intensity 5×10^{14} W/cm^2, FWHM 600 ps, wavelength 0.53 μm) and the aluminum *K*-shell emission (intensity 5×10^{12} W/cm^2, FWHM 600 ps, wavelength 0.53 μm on 3000 Å aluminum target) seen from the Al side as calculated with the TRANSPEC code.

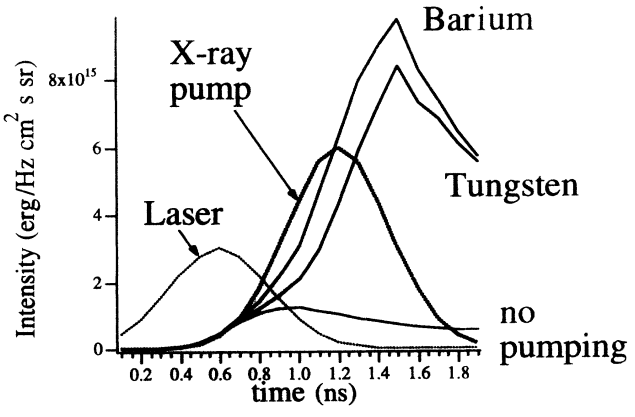

FIG. 6. Space- and frequency-integrated temporal evolution of the He$_\alpha$ line (parallel to the target surface) without pumping and with the two x-ray sources of tungsten and barium as calculated with the TRANSPEC code. The laser pulse creating the Al plasma and the photopumping x-ray source are shown with arbitrary intensity units.

during its rise. Indeed, if the aluminum layer is not completely ablated when photopumping starts, the remaining cold material is able to absorb the x-ray pump at its beginning and limit the fluorescence signal. The difficulty of calculating precisely the ablated thickness of the aluminum layer can then explain the difference between the simulated and experimental time delay of fluorescence rise versus the x-ray pump.

Figure 7(a) shows the spatial distribution of He_α emissivity without and with the photoionization x-ray source at the maximum of the fluorescence. As we expected from the preliminary simulations [17], the fluorescence appears closer to the target surface than self-emission. This is also in accordance with the fact that we had to move back the knife edge from perfect alignment with the target to be able to see the fluorescence signal. It is also in accordance with the fact that, with a too thin aluminum layer (200 nm), we did not see any fluorescence as the optimal region for fluorescence was then located in plastic. The same spatial distribution of He_α emissivity is obtained with the photoexcitation x-ray source. In these two cases, the maximum absorption of the tungsten and barium pumping radiation is located in the first aluminum cells.

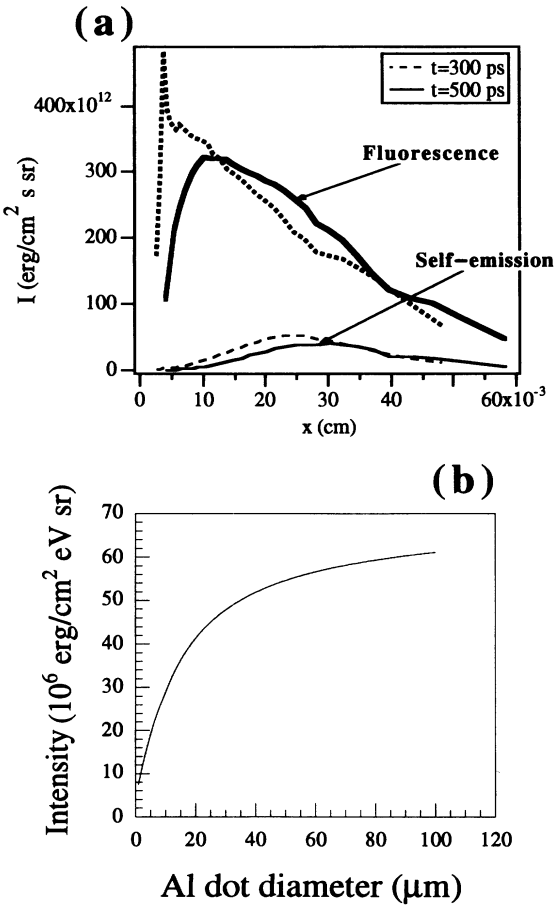

FIG. 7. (a) Frequency-integrated spatial repartition of the He_α line along the laser axis without pumping and with the tungsten x-ray source at two different times after the maximum of the x-ray source as calculated with the TRANSPEC code. (b) Time-integrated He_α line emissivity as a function of aluminum dot diameter as calculated with the TRANSPEC code.

A high reabsorption of the He_α fluorescence signal is to be expected as the fluorescence is occurring in the densest part of the plasma and the oscillator strength of the $1s2p$-$1s^2$ transition is high. To evaluate the reabsorption of this line along the viewing axis, we did some simulations with different aluminum dot diameters in the presence of the photoionization tungsten source. Figure 7(b) shows the time-integrated fluorescence of the aluminum He_α line along the observation axis as a function of the dot diameter. As we can see, a saturation of the emissivity is visible for a plasma diameter greater than 100 μm. This reabsorption explains well the fact that the alignment of the Al dot on the edge of the target was critical during the experiment, as the time-resolved spectrograph could detect only the $1s2p$-$1s^2$ transition optical depth, i.e., less than the 100 to 200 μm diameter of the Al dot.

We have also performed numerical simulations with the one-dimensional radiative hydrocode XRAD to calculate how much heating of the Al layer was expected by the radiative wave and shocks induced by the x-ray source pump [22]. This was an important issue to eliminate other mechanisms of production of He_α emission during the pump laser. The target was a 700 Å tungsten layer deposited onto 10 μm of $(CH)_n$ plastic with a 300 nm aluminum layer on the other side. The two opposite incident laser beam intensities were respectively 5×10^{14} and 5×10^{12} W/cm^2, delayed by 600 ps. The thermal conductivity was described by Spitzer with a 0.03 factor limited heat flux. The absorption coefficients and ionization balance were deduced from a NLTE average-atom model. This code gives a good description of the propagation of the radiative wave but cannot evaluate the fluorescence of the aluminum plasma because the line transfer along the line of sight is not treated. We have compared the obtained electronic temperature of the Al plasma with and without radiative transfer. The enhancement of the temperature during the pump laser is weak, i.e., less than 10 eV. It shows that the radiative wave and shocks are well confined in the 10 μm thick plastic substrate. Also the fluorescence of the line cannot be explained by an alternative heating of the Al plasma, as was confirmed by the counterexperiment described in Sec. IV.

VI. CONCLUSIONS

This paper presents the results of photopumping experiments. Preliminary optimization has been important for the success of the present experiments. It has defined the conditions of creation of the x-ray source and its coupling with the pumped plasma. It has also given the electronic density and temperature that maximize the fluorescence in the aluminum plasma.

The laser-produced x-ray source obtained with a high-Z element has been demonstrated to give efficient photoionization and photoexcitation of a He-like aluminum plasma. Experimental data show clearly the Al He_α line fluorescence due to nonresonant and quasiresonant pho-

topumping. It can be noted that the intensity level of the fluorescence obtained in this experiment is comparable to the fluorescence signal measured in the resonant He-like scheme [4,5]. Thus using a broadband x-ray pump is quite interesting to remove the constraint of line coincidence.

Comparison of the experimental results with radiative-transfer simulations gives a detailed understanding of the physical processes in the pumped plasma. First of all, the simulations show that photopumping is observable and corroborate the behavior of the experimental fluorescence signal. In particular, they confirm that the tungsten photoionizing and the barium photoexciting sources produce comparable fluorescence signals. Second, the simulations show that the volume of plasma from which the fluorescence emerges is spatially restricted to a region closer to the target than the self-emission zone. Finally, the strong reabsorption obtained with the code corroborates the fact that fluorescence was recorded only with aluminum dot targets.

In conclusion, the present work shows that the good comparison between experimental data and the TRANSPEC and FILM code results give a good insight into the physical mechanisms of photopumping. A more detailed comparison would require a better experimental spectral resolution and absolute measurements of the fluorescence signal. The present experiment opens the field of active spectroscopy in which photopumping is used to test complex radiation-transfer codes. Radiative-hydrodynamic simulations of photopumping experiments are a good way to better understand non-LTE radiative transfer in a plasma.

ACKNOWLEDGMENTS

The authors want to thank all the LULI staff, in particular R. Konig for his constant help. They want to thank the Laboratoire des cibles de l'Institut de Physique Nucléaire of Paris XI–Orsay University for collaboration on target design and preparation, and the CDSI of Institut d'Optique in Paris XI–Orsay University for digitizing the films.

[1] N. Qi and M. Krishnan, Phys. Rev. Lett. **59**, 2051 (1987).
[2] P. Monnier, C. Chenais-Popovics, J. P. Geindre, and J. C. Gauthier, Phys. Rev. A **38**, 2508 (1988).
[3] J. L. Porter, R. B. Spielman, M. K. Matzen, E. J. McGuire, L. E. Ruggles, M. F. Vargas, J. P. Apruzese, R. W. Clark, and J. Davis, Phys. Rev. Lett. **68**, 796 (1992).
[4] C. A. Back, R. W. Lee, and C. Chenais-Popovics, Phys. Rev. Lett. **63**, 1471 (1989).
[5] C. A. Back, C. Chenais-Popovics, and R. W. Lee, Phys. Rev. A **44**, 6730 (1991); C. A. Back, J. I. Castor, R. I. Klein, P. G. Dykema, and R. W. Lee, *ibid.* **44**, 6743 (1991).
[6] C. C. Smith, S. J. Davidson, D. J. Hoarty, and J. M. Foster, in *Proceedings of the 4th International Workshop on Radiative Properties of Hot Dense Matter,* edited by W. Goldstein, C. Hooper, J. C. Gauthier, J. Seely, and R. W. Lee (World Scientific, Singapore, 1991), p. 242.
[7] A. V. Vinogradov, I. I. Sobelman, and E. A. Yukov, Kvant. Elektron. (Moscow) **2**, 105 (1975) [Sov. J. Quantum Electron. **5**, 59 (1975)].
[8] E. E. Fill and D. G. Goodwin, in *Soft X-ray Gain in a Plasma Pumped by Photoionization,* edited by M. C. Richardson, SPIE Proc. Vol. 831 (SPIE, Bellingham, WA, 1987), p. 293.
[9] B. N. Chichkov and E. E. Fill, Opt. Commun. **74**, 202 (1989).
[10] R. C. Elton, *X-Ray Lasers* (Academic, San Diego, 1990), pp. 126–145.
[11] B. N. Chichkov and E. E. Fill, Phys. Rev. A **42**, 599 (1990).
[12] H. C. Kapteyn, Appl. Opt. **31**, 4931 (1992).
[13] J. Nielsen, Opt. Commun. **78**, 51 (1990).
[14] T. Boehly, M. Russotto, R. S. Craxton, R. Epstein, B. Yaakobi, L. B. De Silva, J. Nielsen, E. A. Chandler, D. J. Fields, B. J. MacGowan, D. L. Matthews, J. H. Scofield, and G. Shimkaveg, Phys. Rev. A **42**, 6962 (1990).
[15] J. Nielsen, P. Beiersdorfer, S. R. Elliott, and A. L. Osterheld, Phys. Scr. **47**, 42 (1993).
[16] J. P. Apruzese and P. C. Kepple, Phys. Rev. A **43**, 6964 (1991).
[17] C. A. Back, P. Renaudin, C. Chenais-Popovics, and J. C. Gauthier, Laser Part. Beams **10**, 793 (1992).
[18] P. Renaudin, C. A. Back, C. Chenais-Popovics, and J. C. Gauthier, *X-Ray Lasers 1992,* edited by E. E. Fill (IOP, Bristol, 1992), p. 167.
[19] O. Peyrusse, Phys. Fluids B **4**, 2007 (1992); J. Quant. Spectrosc. Radiat. Transfer **51**, 281 (1994).
[20] J. C. Gauthier, J. P. Geindre, N. Grandjouan, and J. Virmont, J. Phys. D **16**, 321 (1983).
[21] J. P. Luciani, P. Mora, and J. Virmont, Phys. Rev. Lett. **51**, 1664 (1983).
[22] J. C. Gauthier and J. P. Geindre, Rapport annuel du LULI, 1987 (unpublished), p. 176, available upon request to the authors.

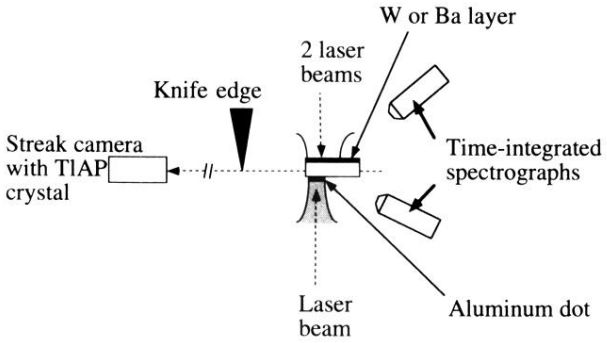

FIG 1. Photopumping experimental geometry. Time-resolved spectrum of the two plasmas are recorded by a streak camera fitted with a thallium hydrogen phthalate (TIAP) flat crystal.

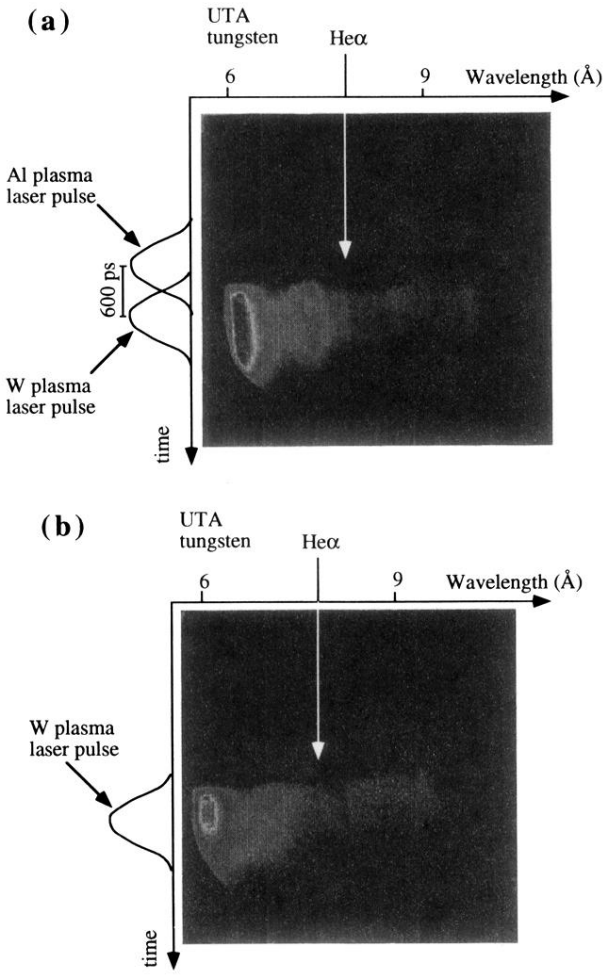

FIG. 3. (a) Time-resolved spectrum of the two plasmas showing the fluorescence of the He_α line; (b) time-resolved spectrum of the tungsten plasma only (laser intensity 10^{14} W/cm^2, FWHM 600 ps, wavelength 0.53 μm).